Interactions between nonlinear resonators represented in Volterra series

David Roze

Interactions between nonlinear resonators represented in Volterra series

David Roze
CNRS, Ircam, Sorbonne Université, Ministère de la Culture,
Sciences et Technologies de la Musique et du Son
STMS lab, 1 place Igor Stravinsky, 75004 Paris, France

Keywords: nonlinear resonators, nonlinear interactions, Volterra series, inverse Volterra kernels

Abstract

This paper aims at introducing nonlinear interactions in the sound synthesis of nonlinear resonators. Sound synthesis is performed using the formalism of Volterra series which is used to describe and simulate weakly nonlinear models using their Volterra kernels. Interactions are constraints imposed to the considered models and are used to excite (e.g. bowing a string or striking a plate) or connect resonators together (such as connecting a string to a bridge). This requires to resolve an inverse problem giving the interaction force as a function of a given velocity.

In the case of Volterra series, kernels of the inverse problem have been defined by Schetzen. Using this definition, a structure of simulation of the direct and inverse problems at each time step will be defined. Application to the case of a Kirchhoff-Carrier string connected to a Berger plate will be presented including computation of the kernels (direct and inverse), structure of simulation and numerical results.

1 Introduction

In the case of sound synthesis based on physical models, we aim to build instruments by connecting resonators using various kinds of interactions. Several approaches have been considered to simulate the dynamics of resonators [1], such as finite differences schemes [2, 3], modal synthesis [4], mass-spring networks [5], digital waveguides [6, 7]. In order to improve realism of the sound synthesis, active research has been done to model and simulate nonlinear resonators to improve sound realism using finite differences scheme[8] the Volterra and Green-Volterra series [9, 10] or the nonlinear normal modes [11].

Virtual instrument making requires to define and solve the coupling between two resonators or between an excitation and a resonator (e.g. a bow, a strike, a reed or lips). For the resonator dynamics this is equivalent to apply a constraint of force or velocity. Recently, numerous works has defined interactions on linear string models using a penalty approach in energy preserving finite-difference scheme [12] [13] [14] [15] [16]. In order to avoid implicit scheme, quadratisation has been proposed to define non iterative schemes [17] [18] [19]. This approach has also been applied to the case of nonlinear resonators [20]. Another recent approach to work with constraints is based on the Udwadia-Kalaba method [21, 22] which has been applied to a beam and string instruments [23] [24] [25]. Lately non-smooth dynamics methods have been used in the field of musical acoustics to work with such interaction problems [26].

https://doi.org/10.1016/j.jsv.2021.116590

This paper focuses on solving constraints applied to resonators represented by their Volterra kernels. This formalism allows to compute the dynamics of weakly nonlinear systems. Structure of simulations with low computation cost has been proposed in [9],[10]. The aim is to propose a generic non-iterative formalism based on the definition of inverse Volterra kernels made by Schetzen [27]. That is, solving the inverse problem in the case of weakly nonlinear dynamics. This result will be used to propose a structure of simulation that will lead to the possibility to apply constraints in the dynamics of nonlinear physical models and will allow a wide range of interactions such as adherence, strike, blow, or a bow with a chosen friction law. Applications of these results will be presented with simples cases: (i) a shortened string (e.g case of a finger imposing a zero velocity at one point of the string), (ii) collision of a string with a barrier, (iii) a bowed string and (iv) a string coupled to a plate in one point (simplification of the interaction between a string and a plate through a bridge [28]).

Section 2 will provide reminders on nonlinear wave propagation in the Volterra series formalism with the example of the Berger plate model Volterra kernels. Section 3 will define interactions based on Volterra series, using Schetzen result on the kernels of the inverse system. Finally, section 4 will describe a numerical implementation and present results of simulation.

2 Nonlinear wave propagation simulation

Volterra series [29, 30] have been used to compute dynamics of weakly nonlinear systems. This extension of the convolution is based on Volterra kernels that can be identified from a (partial) differential equation or measured. This section will remind the computation of the direct problem with the example of the Berger plate model. These results will be used to define interactions between nonlinear resonators based on their inverse Volterra kernels, in section 3.

2.1 Reminder on Volterra series

Definition 1 (Volterra series) *A system with input $f(t)$ and output $u(t)$, defined on domain $\mathbb{T}$, is described by a Volterra series of kernels $\{h_n\}_{n\in\mathbb{N}^*}$ (see Fig. 1), if*

$$u(t) = \sum_{n=1}^{+\infty} \int_{\mathbb{T}^n} h_n(\boldsymbol{\tau}) f(t-\tau_1)\dots f(t-\tau_n)\mathrm{d}\boldsymbol{\tau}, \tag{1}$$

where, for each $n \in \mathbb{N}^*$, bold symbol $\boldsymbol{\tau}$ denotes (in each kernel h_n, without ambiguity) the n-tuple $\boldsymbol{\tau}=(\tau_1,\dots,\tau_n)$, and where $\mathrm{d}\boldsymbol{\tau}$ is the corresponding Lebesgue measures.

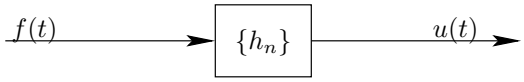

Figure 1: System represented by its Volterra kernels.

The multivariate Laplace transform of Volterra kernels

$$H_n(s_1,\dots,s_n) = \int_{\mathbb{T}^n} h_n(\tau_1,\dots,\tau_n)\mathrm{e}^{-(s_1\tau_1+\dots+s_n\tau_n)}\mathrm{d}\boldsymbol{\tau},$$

defines the transfer kernels which generalise transfer functions.

Interconnection laws Interconnection laws allows to compute the equivalent kernels (in time or Laplace domain) in the three cases described in Fig. 2.

In the Laplace domain, theses three cases lead to (see [10] for the time version equivalents):

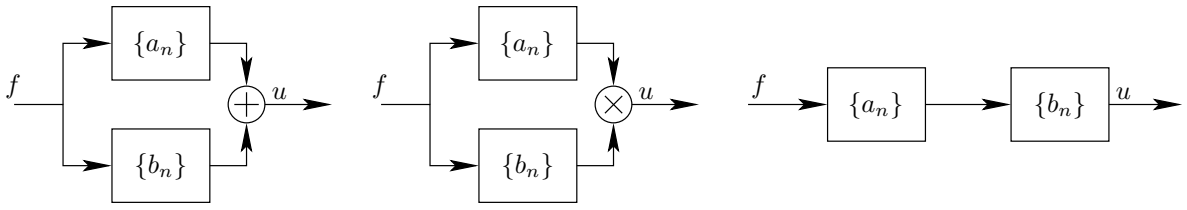

(a) Sum **(b) Product** **(c) Cascade with a linear operator**

Figure 2: *Interconnection laws of several Volterra systems: (a) sum, (b) product, (c) cascade with a linear operator.*

- Sum:
$$H_n(s_1, \ldots, s_n) = A_n(s_1, \ldots, s_n) + B_n(s_1, \ldots, s_n); \tag{2}$$
- Product
$$H_n(s_1, \ldots, s_n) = \sum_{p=1}^{n-1} A_p(s_1, \ldots, s_p) B_{n-p}(s_{p+1}, \ldots, s_n); \tag{3}$$
- Cascade with a linear operator B ($B_1 \neq 0$ and $B_n = 0$ if $n \neq 1$):
$$H_n(s_1, \ldots, s_n) = A_n(s_1, \ldots, s_n) B_1(s_1 + \cdots + s_n). \tag{4}$$

For further clarity, $(s_1, \ldots, s_n)$ will be denoted $\boldsymbol{s}$ and $(s_1 + \cdots + s_n)$ will be denoted $\widehat{\boldsymbol{s}}_{1:n}$.

2.2 The Berger plate model

The Berger plate model [31] describes the transverse displacement of a weakly nonlinear plate and can be seen as the equivalent of the Kirchhoff-Carrier string model for the plate (its nonlinearity consists in a tension modulation due to the large deflections). It is defined by

$$\rho H \frac{\partial^2 u(t,x,y)}{\partial t^2} = -D\Delta\Delta u(t,x,y) + \left(\frac{6D}{\mathcal{A}H^2} \int_{\mathcal{D}} |\nabla u(t,x,y)|^2 \mathrm{d}x\mathrm{d}y \right) \Delta u(t,x,y) - \rho H \sigma \frac{\partial u(t,x,y)}{\partial t} + f(t,x,y), \tag{5}$$

with ρ the plate density (kg m^{-3}), H its thickness (m), $D = \frac{EH^3}{12(1-\nu^2)}$ the flexural rigidity (N m), $\mathcal{A} = L_x L_y$ the plate area (m^2), σ the fluid damping (s^{-1}) and $f(t,x,y) = \phi(x,y)F(t)$ the excitation force (N m^{-2}).

The plate is at rest for $t \leq 0$ and simply supported on its edges:

$$\begin{aligned}
\forall (x,y) \in \mathcal{D}_y = \{0; L_x\} \times [0, L_y] \qquad & u(x,y,t) = \frac{\partial^2 u(x,y,t)}{\partial y^2} = 0, \\
\forall (x,y) \in \mathcal{D}_x = [0, L_x] \times \{0; L_y\} \qquad & u(x,y,t) = \frac{\partial^2 u(x,y,t)}{\partial x^2} = 0, \\
\forall (x,y) \in \mathcal{D} = [0, L_x] \times [0, L_y], \forall t \in \mathbb{R}^- \qquad & u(x,y,t) = 0.
\end{aligned}$$

Remark on the Berger plate model The Kirchhoff-Carrier string model and the Berger plate model are nonlinear models describing the behaviour of one degree of freedom (transverse displacement). They obviously neglect the other degrees of freedom and the coupling between them, which is a source of inaccuracy. However, these models can be valid up to a certain point (cf. [32] for the Berger plate model) and can be used in the field of sound synthesis where they allow to retrieve classical nonlinear phenomena (frequency variation, etc.). Therefore, they can be seen as good examples to introduce the results of this paper without using full beam or plate models.

2.2.1 Dimensionless model

In order to simplify computation of the Volterra kernels, the dimensionless version of Eq. (5) will be considered with the following variables: $\tilde{t} = \frac{t\alpha}{L_x L_y}$ (with $\alpha = \sqrt{\frac{D}{\rho H}}$), $\tilde{x} = \frac{x}{L_x}$, $\tilde{y} = \frac{y}{L_y}$ and $u(t,x,y) = U^\star \tilde{u}(\tilde{t},\tilde{x},\tilde{y})$. Omitting tilda for sake of legibility, the dimensionless model writes

$$\frac{\partial^2 u(t,x,y)}{\partial t^2} = -\Delta\Delta u(t,x,y) + \left(\psi \int_{\mathcal{D}_0} |\nabla u(x,y,t)|^2 \mathrm{d}x\mathrm{d}y\right) \Delta u(t,x,y) - \delta \frac{\partial u(t,x,y)}{\partial t} + \phi(x,y)F(t), \quad (6)$$

with $\lambda = \frac{L_x}{L_y}$, $\delta = \frac{L_x L_y \sigma}{\alpha}$, $\frac{6(U^\star)^2}{H^2} = \psi$, and the differential operators $\nabla = \begin{bmatrix} \frac{1}{\sqrt{\lambda}}\frac{\partial}{\partial x} \\ \sqrt{\lambda}\frac{\partial}{\partial y} \end{bmatrix}$ and $\Delta = \frac{1}{\lambda}\partial_x^2 + \lambda\partial_y^2$.

2.3 Volterra kernels of the dimensionless Berger plate model

Using the cancelling system method and modal decomposition Volterra kernels of the Berger plate model are defined by (see B for more details):

$$H_n^{[kl]}(\boldsymbol{s}) = Q^{[kl]}(\boldsymbol{s}) E_n^{[kl]}(\boldsymbol{s}),$$

with

$$\begin{aligned} Q^{[kl]}(\boldsymbol{s}) &= \left(\widehat{\boldsymbol{s}}_{1:n}^2 + \delta\widehat{\boldsymbol{s}}_{1:n} + \frac{k^4\pi^4}{\lambda^2} + \lambda^2 l^4\pi^4 + 2k^2 l^2 \pi^4\right)^{-1}, \\ E_1^{[kl]}(s) &= \langle \phi, e_{kl} \rangle (x,y), \end{aligned}$$

and

$$\begin{aligned} E_n^{[kl]}(\boldsymbol{s}) &= \psi \left\langle \int_{\mathcal{D}} \sum_{p,q,r} \left(\frac{1}{\lambda}\frac{\partial H_p^{(x,y)}}{\partial x}\frac{\partial H_q^{(x,y)}}{\partial x} + \lambda \frac{\partial H_p^{(x,y)}}{\partial y}\frac{\partial H_q^{(x,y)}}{\partial y}\right) \mathrm{d}x\mathrm{d}y \right. \\ &\qquad \left. \left(\frac{1}{\lambda}\frac{\partial^2 H_r^{(x,y)}}{\partial x^2} + \lambda \frac{\partial^2 H_r^{(x,y)}}{\partial y^2}\right), e_{kl} \right\rangle, \\ E_n^{[kl]}(\boldsymbol{s}) &= -\psi\pi^4 \left(\frac{k^2}{\lambda} + l^2\lambda\right) \sum_{p,q,r} \sum_{(m,n)} H_p^{[mn]} H_q^{[mn]} \left(\frac{m^2}{\lambda} + n^2\lambda\right) H_r^{[kl]}, \\ E_n^{[kl]}(\boldsymbol{s}) &= \gamma_{kl} \sum_{p,q,r} \sum_{(m,n)} H_p^{[mn]} H_q^{[mn]} \left(m^2 + n^2\lambda^2\right) H_r^{[kl]}, \end{aligned}$$

with $\gamma_{kl} = \psi \frac{-\pi^4(k^2 + l^2\lambda^2)}{\lambda^2}$.

2.4 Structure of simulation

The structure of simulation based on Volterra kernels up to order 3 is presented in Fig. 3. Simulation of each filter

$$Q^{[kl]}(\boldsymbol{s}) = \left(\widehat{\boldsymbol{s}}^2 + \delta\widehat{\boldsymbol{s}} + \frac{k^4\pi^4}{\lambda^2} + \lambda^2 l^4\pi^4 + 2k^2 l^2\pi^4\right)^{-1},$$

is based on the formulation presented in A.1 with

$$\mathbf{A}^{[kl]} = \begin{bmatrix} 0 & 1 \\ \left(\frac{k^4}{\lambda^2} + l^4\lambda^2 + 2k^2 l^2\right)\pi^4 & -\delta_{kl} \end{bmatrix}.$$

The solution up to order 3 writes $\mathbf{X}(t_i,x,y) = \mathbf{X}_1(t_i,x,y) + \mathbf{X}_3(t_i,x,y)$ with

$$\begin{aligned}
\mathbf{X}_1(t_i,x,y) &= \sum_{k=1}^{K}\sum_{l=1}^{K} \tilde{\mathbf{X}}_1^{[kl]}(t_i)e_{kl}(x,y) + \mathbf{B}_\phi^{[kl]}F^{[kl]}(t_i)e_{kl}(x,y), \\
&= \sum_{k=1}^{K}\sum_{l=1}^{K} \mathrm{e}^{\mathbf{A}^{[kl]}t_s}\mathbf{X}_1^{[kl]}(t_{i-1})e_{kl}(x,y) + \mathbf{B}_\phi^{[kl]}F^{[kl]}(t_i)e_{kl}(x,y), \qquad (7) \\
F_3^{[kl]}(t_i) &= \sum_{p=1}^{K}\sum_{q=1}^{K} \left(p^2+q^2\lambda^2\right)\left(\mathbf{X}_1^{[pq]}(t_{i-1})\right)^2 \mathbf{X}_1^{[kl]}(t_{i-1}), \qquad (8) \\
\mathbf{X}_3(t_i,x,y) &= \sum_{k=1}^{K}\sum_{l=1}^{K} \tilde{\mathbf{X}}_3^{[kl]}(t_i)e_{kl}(x,y) + \gamma_{kl}\mathbf{B}_0^{[kl]}F_3^{[kl]}(t_i)e_{kl}(x,y), \\
&= \sum_{k=1}^{K}\sum_{l=1}^{K} \mathrm{e}^{\mathbf{A}^{[kl]}t_s}\mathbf{X}_3^{[kl]}(t_{i-1})e_{kl}(x,y) + \gamma_{kl}\mathbf{B}_0^{[kl]}F_3^{[kl]}(t_i)e_{kl}(x,y), \qquad (9)
\end{aligned}$$

with $\mathbf{B}_0^{[kl]} = -\mathbf{A}^{[kl]^{-1}}\left(\begin{bmatrix}0\\1\end{bmatrix} - \mathrm{e}^{\mathbf{A}^{[kl]}t_s}\begin{bmatrix}0\\1\end{bmatrix}\right)$ and $\mathbf{B}_\phi^{[kl]} = \phi^{[kl]}\mathbf{B}_0^{[kl]}$ for an excitation force defined as $f(x,t) = \phi(x)F(t)$.

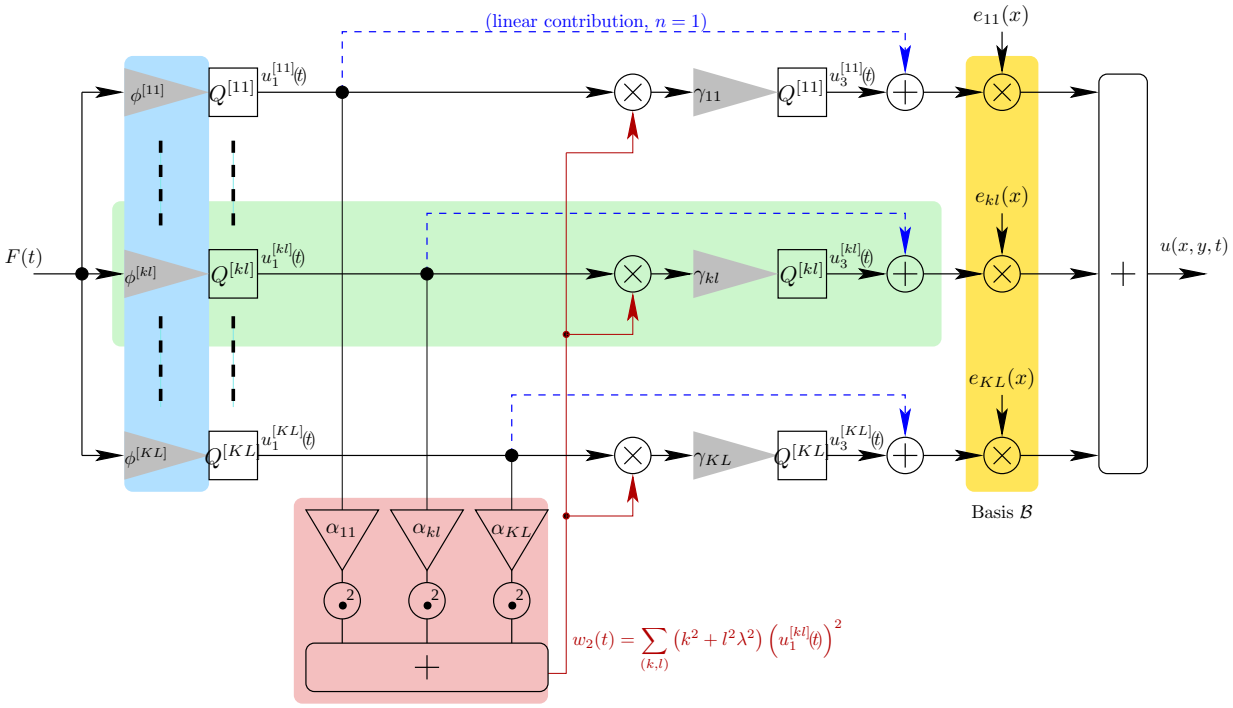

Figure 3: Structure of simulation of the dimensionless Berger plate model (cf. Eq. (6)) up to order 3 using Volterra kernels. q^{kl} are the filters computing the modal dynamics for each pair of modes (k,l).

3 Interactions based on Volterra series

In this work, interactions will be seen as constraints imposed to the considered resonator. This constraint will be seen as an imposed velocity or displacement and allow to define many interactions.

3.1 Generic interaction definition

In the case of linear resonators (cf. Eq. (20)) computation of the dynamics

$$\mathbf{CX}(x,t) = \mathbf{C}\tilde{\mathbf{X}}(x,t)+) \sum_k \mathbf{CB}_\phi^{[k]} F(t) e_k(x), \tag{10}$$

where $\mathbf{C}$ is a row vector to select displacement or velocity, allow to compute an interaction force to impose a given displacement or velocity at point x_I:

$$F_I(t) = \frac{\mathbf{CX}(x_I,t) - \mathbf{C}\tilde{\mathbf{X}}(x_I,t)}{\sum_k \mathbf{CB}_\phi e_k(x_I)}. \tag{11}$$

In the case of a nonlinear resonator described by it Volterra kernels up to order N (cf. Eqs. (7-9)), the computation of F_I require the inverse Volterra kernels of the system since the equivalent equation of Eq. (10) is a Nth-order polynomial of the interaction force.

Following the definition of the inverse kernels in the next subsection, we will propose an algorithm to compute the interaction force required to impose a desired velocity at the same point, this will allow to define several application examples in section 4.

3.2 Kernels of the inverse system: definition

Definition 2 (cf. [27]) *The inverse Volterra series $\{K_n\}$ of a nonlinear system represented by its Volterra kernels $\{H_n\}$, is defined such as the cascade of $\{H_n\}$ and $\{K_n\}$ is the identity application until a given order (cf. Fig. 4).*

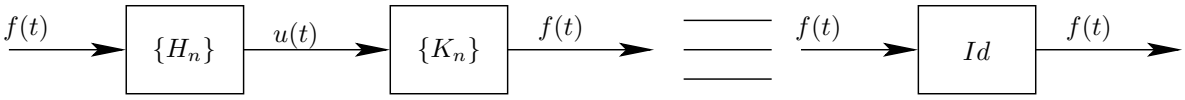

Figure 4: Definition of the inverse of a system represented by its Volterra series.

In the Laplace domain, the equivalent kernels $\{C_n\}$ of the cascade of $\{H_n\}$ and $\{K_n\}$ are defined by (cf. e.g. [33, 29])

$$\begin{aligned} C_n(s_1,\ldots,s_n) &= \sum_{m=1}^{n} \sum_{\substack{p\in\mathbb{N}^\star \\ p_1+\cdots+p_m=n}} K_m(s_1+\cdots+s_{p_1},\ldots,s_{p_1+\cdots+p_{m-1}+1}+\cdots+s_n) \\ &\quad H_{p_1}(s_1,\ldots,s_{p_1})\ldots H_{p_m}(s_{p_1+\cdots+p_{m-1}+1},\ldots,s_n). \end{aligned}$$

Following the procedure proposed by Schetzen in Definition 2, inverse kernels $\{K_n\}$ are found knowing that $C_1(s_1) = 1$ and $\forall n \geq 2$, $C_n(s_1,\ldots,s_n) = 0$, leading to the following results for the three first orders

$$K_1(s) = (H_1(s))^{-1}, \tag{12}$$

$$K_2(s_1,s_2) = -K_1(s_1+s_2)H_2(s_1,s_2)K_1(s_1)K_1(s_2), \tag{13}$$

$$\begin{aligned} K_3(s_1,s_2,s_3) &= -K_1(s_1+s_2+s_3)H_3(s_1,s_2,s_3)K_1(s_1)K_1(s_2)K_1(s_3), \\ &\quad -K_2(s_1+s_2,s_3)H_2(s_1,s_2)H_1(s_3)K_1(s_1)K_1(s_2)K_1(s_3), \\ &\quad -K_2(s_1,s_2+s_3)H_1(s_1)H_2(s_2,s_3)K_1(s_1)K_1(s_2)K_1(s_3). \end{aligned} \tag{14}$$

- The first inverse kernel K_1 consists in solving the inverse linear problem, which in our case is equivalent to the formulation of Eq. (11).
- Extension of this result to the nonlinear case consists in the simulation of kernels K_n which are iteratively defined using lower order kernels (cf. Eqs. (12-14) and Fig. 5).

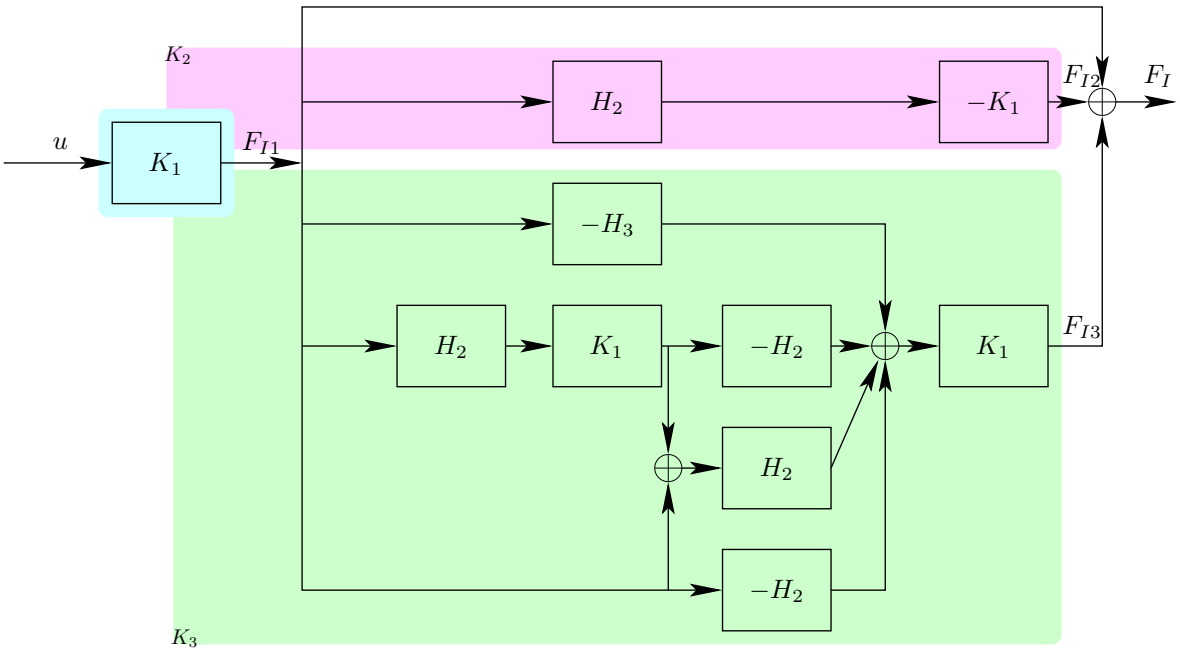

Figure 5: Simplified form of Volterra kernels of the inverse system up to order 3 computed by Schetzen [27].

3.3 General formulation of the inverse

3.3.1 Case of constraint on one resonator

The interaction definition introduced in A.2 can be extended to the nonlinear case until a given order N (in this paper we will consider $N = 3$). The input v_0 is the desired velocity at a given point x_I and the output $F_I = F_{I1} + F_{I2} + F_{I3}$ is the sum of the outputs of the inverse kernels K_1, K_2 and K_3 defined in Eqs. (12-14) and Fig. 5.

A displacement or velocity constraint in one point is therefore computed using the following procedure detailed in algorithm 1:

A Simulation of the direct problem (H_1, H_2 and H_3) with the known forces f (cf. Eqs. (7)-(9)).

B Solve the linear inverse problem K_1 (cf. Eq. (11)) to impose the given velocity v_0.

C Solve the second (K_2) and third order (K_3) inverse problem using F_{I1} as input (cf. Fig. 5) to find the order 2 and order 3 interaction forces F_{I2} and F_{I3}.

D Compute dynamics of the direct problem with the known forces and the interaction forces.

Applications results will be presented in section 4 for different interactions.

3.3.2 Case of interaction between two resonators

Many interactions between two resonators can be defined using the relative velocity between the interaction points

$$v_r = v_s(x_{Is}, t) - v_p(x_{Ip}, y_{Ip}, t),$$

where v_r is the relative velocity between the string at point interaction point x_{Is} and the plate at the interaction point (x_{Ip}, y_{Ip}).

Algorithm 1

A. Simulation of the direct problem with the known forces (cf. Eqs. (7)-(9)).

$$\begin{aligned}
\mathbf{X}_1(x_i,t_{h+1}) &= \sum_{k=1}^{K}\left(\mathrm{e}^{\mathbf{A}^{[k]}t_s}\mathbf{X}_1^{[k]}(t_h)+\mathbf{B}_{\phi}^{[k]}F(t_{h+1})\right)e_k(x_i),\\
\mathbf{X}_2(x_i,t_{h+1}) &= \sum_{k=1}^{K}\left(\mathrm{e}^{\mathbf{A}^{[k]}t_s}\mathbf{X}_2^{[k]}(t_h)+\mathbf{B}_{NL2}^{[k]}F_2(t_{h+1})\right)e_k(x_i),\\
\mathbf{X}_3(x_i,t_{h+1}) &= \sum_{k=1}^{K}\left(\mathrm{e}^{\mathbf{A}^{[k]}t_s}\mathbf{X}_3^{[k]}(t_h)+\mathbf{B}_{NL3}^{[k]}F_3(t_{h+1})\right)e_k(x_i).
\end{aligned}$$

B. Solve the linear inverse problem (K_1, cf. Eq. (21)) to impose the given velocity v

$$F_{I1}(t_{h+1}) = \frac{v-\mathbf{C}\sum_{k=1}^{K}\mathrm{e}^{\mathbf{A}^{[k]}t_s}\mathbf{X}^{[k]}(t_h)e_k(x_i)}{\mathbf{C}\sum_{k=1}^{K}\mathbf{B}_I^{[k]}e_k(x_i)}.$$

C. Solve the second and third order inverse problem by computing the second and third kernel outputs F_{I2} and F_{I3} using F_{I1} as input (cf. Fig. 6).

D. Compute dynamics of the direct problem with the known forces and the interaction force $F_I = F_{I1}+F_{I2}+F_{I3}$

$$\begin{aligned}
\mathbf{X}_1(x_i,t_{h+1}) &= \sum_{k=1}^{K}\left(\mathrm{e}^{\mathbf{A}^{[k]}t_s}\mathbf{X}_1^{[k]}(t_h)+\mathbf{B}_{\phi}^{[k]}F(t_{h+1})+\mathbf{B}_I^{[k]}F_I(t_{h+1})\right)e_k(x_i),\\
\mathbf{X}_2(x_i,t_{h+1}) &= \sum_{k=1}^{K}\left(\mathrm{e}^{\mathbf{A}^{[k]}t_s}\mathbf{X}_2^{[k]}(t_h)+\mathbf{B}_{NL2}^{[k]}F_2(t_{h+1})\right)e_k(x_i),\\
\mathbf{X}_3(x_i,t_{h+1}) &= \sum_{k=1}^{K}\left(\mathrm{e}^{\mathbf{A}^{[k]}t_s}\mathbf{X}_3^{[k]}(t_h)+\mathbf{B}_{NL3}^{[k]}F_3(t_{h+1})\right)e_k(x_i).
\end{aligned}$$

In the nonlinear case simulation will stay similar to the case of a single resonator since it relies on the procedure described previously (in section 3.3.1) where each step is performed for each resonator, except for the linear inverse problem of step B where K_1 is computed for both resonators

$$F_{I1}(t_{h+1}) = \frac{v_{r0} - \tilde{v}_r}{\mathbf{CB}_{Is}(x_{Is}) + \mathbf{CB}_{Ip}(x_{Ip}, y_{Ip})} = \frac{v_{r0} - \mathbf{C}\tilde{\mathbf{X}}_{\mathbf{s}}(x_{Is}, t_h) + \mathbf{C}\tilde{\mathbf{X}}_{\mathbf{p}}(x_{Ip}, t_h)}{\mathbf{CB}_{Is}(x_{Is}) + \mathbf{CB}_{Ip}(x_{Ip}, y_{Ip})},$$

with the desired relative velocity v_{r0} as input and knowing that $F_{Is} = -F_{Ip}$.

Application will be presented in section 4.4.

4 Application to different interactions

Simulation of the string and the plate models has been performed with the physical parameters described in table 1.

The excitation force $f(x,t) = \phi(x)F(t)$ is defined by

$$\phi(x) = \phi_{\max} \cos(\pi \frac{x - x_0}{l}) 1_{[x_0 - \frac{l}{2}, x_0 + \frac{l}{2}]}(x), \quad (15)$$

$$F(t) = F_{\max} \frac{t}{T} 1_{[0,T]}(t), \quad (16)$$

where $x_0 = 0.37L$ is the excitation point, $l = 0.04L$ is the width on which the force is applied and $T = 10^{-2}$ s.

	Young modulus	Poisson ratio	Dimensions	First eigenfrequencies
String	200 GPa	0.3	1.8 m	55 Hz, 110 Hz, 165 Hz...
Plate	40 GPa	0.3	1.2×1.2 m^2	15 Hz, 37 Hz, 60 Hz...

Table 1: Physical parameters of the string and plates used in the simulation.

In the case of the Kirchhoff-Carrier string model and Berger plate model, the even order Volterra kernels are zero, the inverse kernels computation presented in Fig. 5 is simplified as shown in Fig. 6.

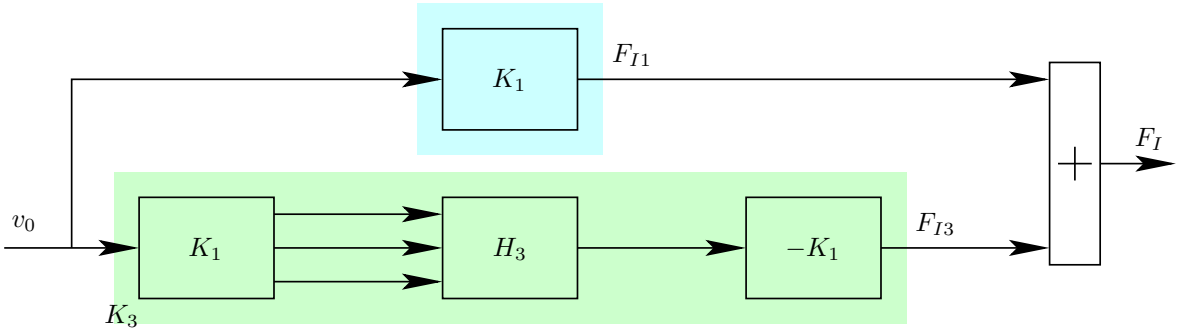

Figure 6: Volterra kernels of the inverse system up to order 3 for the Kirchhoff-Carrier string model and the Berger plate model (where kernel H_2 and therefore its inverse K_2 equal zero).

4.1 Velocity constraint at one point of a string

The case of a velocity constraint v_0 at one point of the string is solved using the general algorithm 1 which is represented by the block-diagram of Fig. 7. In the case of an imposed zero velocity, this can represent a finger shortening a string by pressing it on a fingerboard.

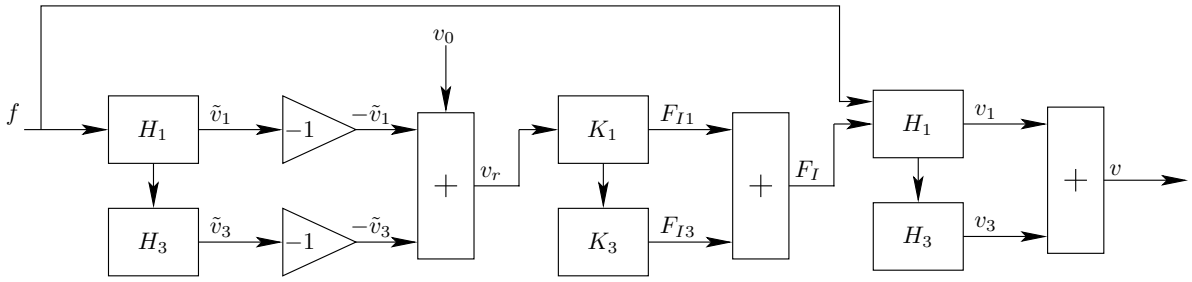

Figure 7: Block-diagram of the computation of the dynamics of a system represented by its Volterra kernels H_1 and H_3. Velocity v_0 is imposed at one point. The difference of velocities $v_r = v_0 - (\tilde{v}_1 + \tilde{v}_3)$ is the input of the inverse problem described by kernels K_n. The interaction force F_I computed is applied to the string in addition to the known force f in order to respect the interaction.

After excitation by the force (15-16), the string vibrates freely. Then, a zero velocity is imposed at the point $x_I = 0.7L$ at time $t = 0.2$ s during 0.3 s, shortening the vibrating part of the string.

The velocity signals at the interaction point x_I can be seen on Fig. 8 for respectively, the first order output $v_1(x_I, t)$, the third order output $v_3(x_I, t)$ and their sum. The first order is the output of the first order kernel H_1, i.e. the response of the linearised system. The second line is the output of the third order kernel H_3 (first order of nonlinearity) and therefore represent the order 3 contribution of the dynamics alone. In this paper, the Volterra series is limited to order $N = 3$. Using the definition of Volterra series in Eq. (1) the approximated output of the system is therefore the sum of the two first lines.

Using the definition of the inverse Volterra kernels by Schetzen [27] and the algorithm presented in section 3.3, the zero velocity constraint is successfully applied until a given order $N = 3$ at the interaction point, which can be verified on the last line of Fig. 8. The interaction force acts mainly on the dynamics of the linear response and have a more subtle effect on the order 3 output. However when the interaction is released at time $t = 0.5$ s both signals are modified with higher frequency content by the new dynamics that was introduced. It can be seen on Figs. 8 and 9b that the amplitude of order 3 is smaller that for the linear response. This lower amplitude when the nonlinear order increases can be used as a first indication of the Volterra series convergence which will not be studied in this paper.

The shortening of the string is illustrated by spectrogram of Fig. 9a where the frequencies increase when the interaction is imposed (from 55 to 79 Hz for the first mode, which is the fundamental frequency of a string for a length of $0.7L$ with the same tension). During the interaction (from 0.2 to 0.7 s) new modes of the shortened string can be seen on the magnitude of the spectrum and the spectrogram presented in Fig. 9. When the interaction is released we can see the amplitudes of the initial modes have been modified by the new ones during the interaction. Moreover, modes of the other part of the string which have a length of $0.3L$ (fundamental frequency of 183 Hz) can be seen with a lower intensity.

Following the same idea, simulation of a glissando (continuous variation of the playing frequency by moving a finger shortening a string for example) has been performed by moving the interaction along string (from the initial point $x_I = 0.7L$ to $0.4L$) during the simulation. Result can be seen on the spectrograms in Fig. 10 for the observation point $x = 0.17L$ where frequencies increase during the shortening of this part of the string. In the same time, decreasing frequencies can be observed for the observation point $x = 0.9L$ located in the other part of the string. As in the previous case of a non-moving constraint, spectrograms of each vibrating part reveal frequencies of the other vibrating part of the string showing that the interaction does not fully split the string into two isolated strings.

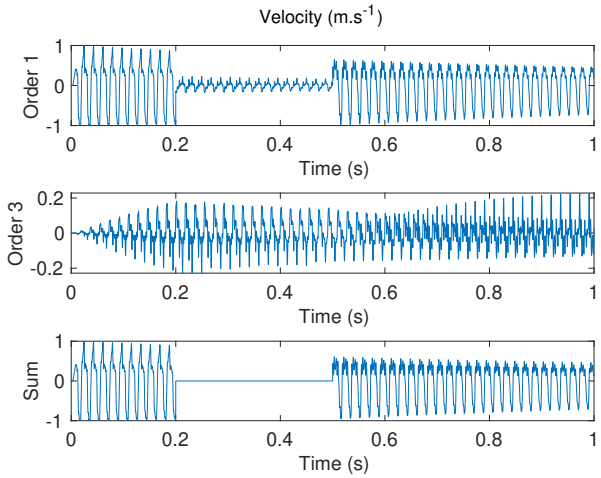

Figure 8: String velocity of the string at the interaction point $x_{Is} = 0.7L$ for orders 1, order 3 and their sum. When the interaction is applied the total velocity is zero.

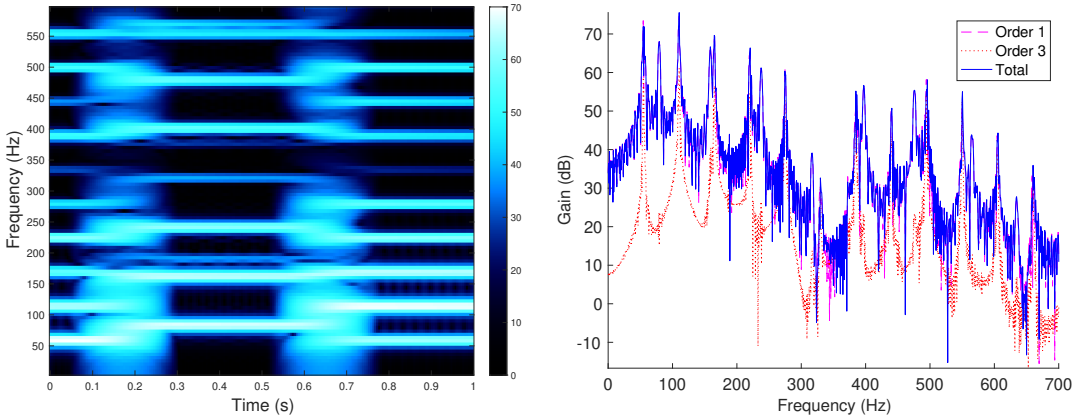

(a) Spectrogram of the velocity signal at point $x_{obs} = 0.17L$.

(b) Spectrum of the velocity signal at point $x_{obs} = 0.17L$.

Figure 9: The interaction shortening the string is visible when the frequencies increase. On the spectrum the modes of the string are visible at frequencies multiple of 55 Hz and the shifting for the shortened string is visible around 79 Hz and multiples.

4.2 Collision of a vibrating string with a barrier

Simulation is performed using the parameters in table 1 for the string model and the excitation force defined in Eqs. (15-16). In this case, the vibration is modified by the presence of rigid barrier located at point $x_I = 0.7L$ and at a distance $u_0 = 1.5$ mm below the string at rest.

Computation is done using the same method that in section 4.1 but with a displacement constraint at the position of the barrier. If the string displacement at point x_I is larger (in absolute value) or equal to u_0, contact is assumed and a displacement constraint of value u_0 is applied involving the computation of a reaction force.

Fig. 11 shows the string transverse displacement at several time steps before and after the two first collisions of the string with the barrier at point x_I. The simulation reveals that the presence of the barrier is globally taken into account in the string dynamics. However it can be noticed that

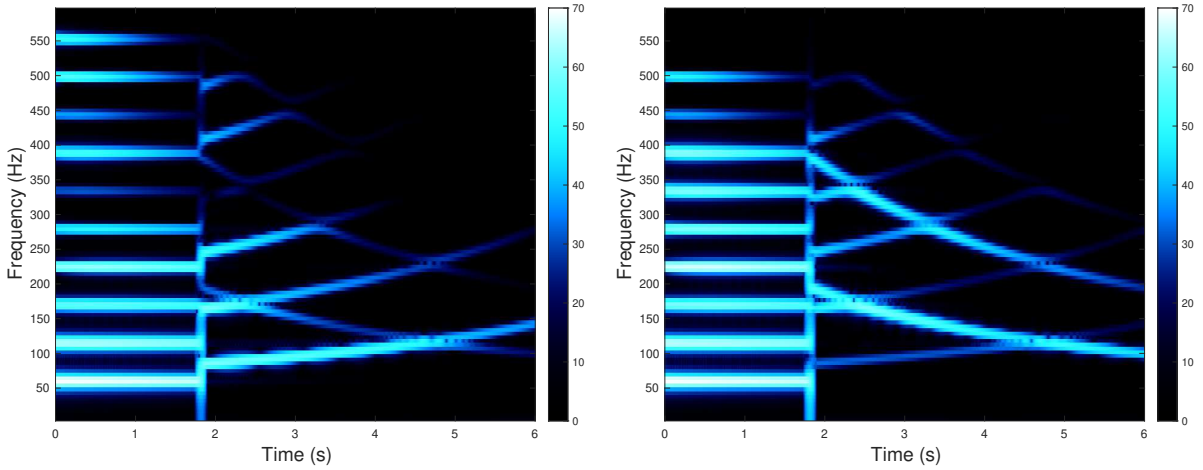

Figure 10: Spectrograms of the string velocity signal at the observation points $x_{obs} = 0.17L$ and $x_{obs} = 0.9L$. After the interaction is imposed, the interaction point moves from $0.7L$ to $0.4L$.

the displacement constraint is not exactly respected and interpenetration can be observed with a displacement slightly below the barrier position during some contacts. This can be related to the fact that starting from the second collision, high frequency oscillations appear near the interaction point. This is related to the discontinuity of the interaction force which can be seen in Fig. 13. These discontinuities should be handled with another approach based on non-smooth mechanics such as described in e.g. [34][26].

Displacement of the string at interaction point is represented in Fig. 12 for the first order, third order and their sum. The contact with the barrier can be seen on the last line when the transverse displacement is limited to -1.5 mm with the exception of few interpenetrations during some collisions. This interaction induced modification in the waveform between 0 and 0.16 s in both order 1 and order 3 responses when the amplitude of the string vibration is large enough to reach the barrier.

4.3 Bowed string

The formalism presented in section 3.3.1 can be applied to compute the motion of a bowed string.

The string is excited by a bowing force F_I which follows the characteristics (see e.g. [3])

$$F_I(v_r) = \sqrt{2a} F_B v_r e^{-a v_r^2 + 0.5}, \tag{17}$$

where F_B is the normal force, a a parameter of the model and v_r the relative velocity between the bow and the string at the bowing point x_I.

Simulations results are presented in Fig. 14 for $F_B = 1$ N, a bowing velocity $v_B = 0.1$ m s^{-1}, $x_I = 0.25L$ m and $a = 100$ s^2 m^{-2}. Self-oscillations of the transverse displacement emerges quickly. A zoom on the displacement reveals the expected sawtooth waveshape in the linear response. The third order response is one order of magnitude lower and has a completely different waveshape with a positive almost constant value during the sticking phase ($v_r = 0$) and a negative one during the sliping phase ($v_r > 0$). As in the displacement case, the expected waveform of the relative velocity is visible in the linear response with the alternance between stick and slip phases. The third order response is lower but within the same order of magnitude. The third order velocity response ($v = v_B - v_r$ with $v_B = 0.1$ m s^{-1}) is zero during the sticking phase, have a negative value at the beginning of the slipping phase and a positive one at the end of it.

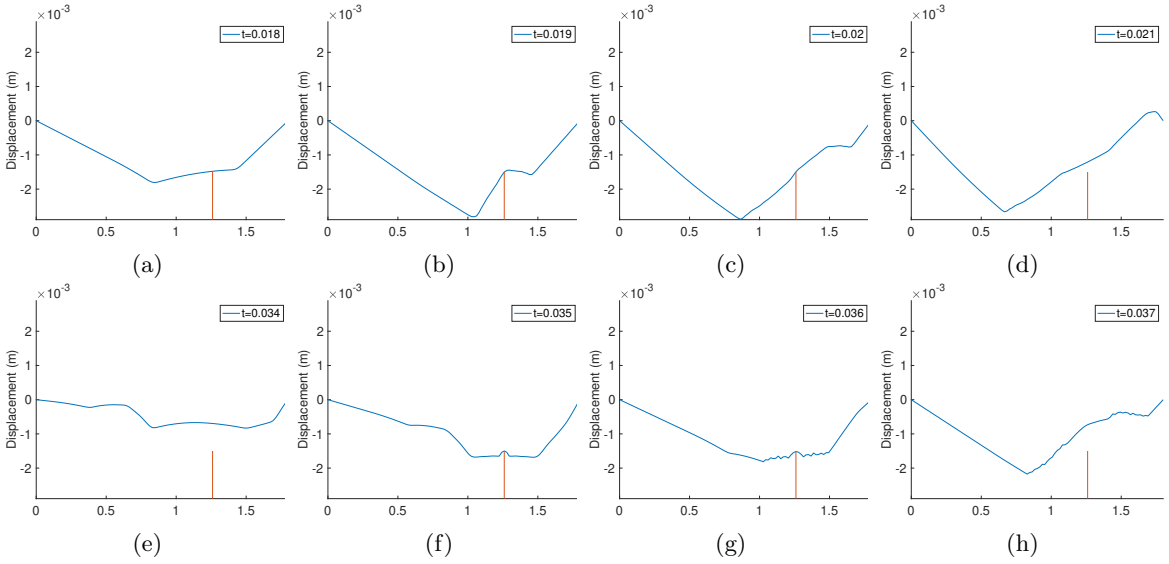

Figure 11: Transverse displacement of the whole string at different time steps. Collision with the barrier located at $x_I = 0.7L$ is visible on plots (c-d) and (f-g). (a-d) First collision. (e-h) Second collision with presence of high frequency oscillations around the interaction point.

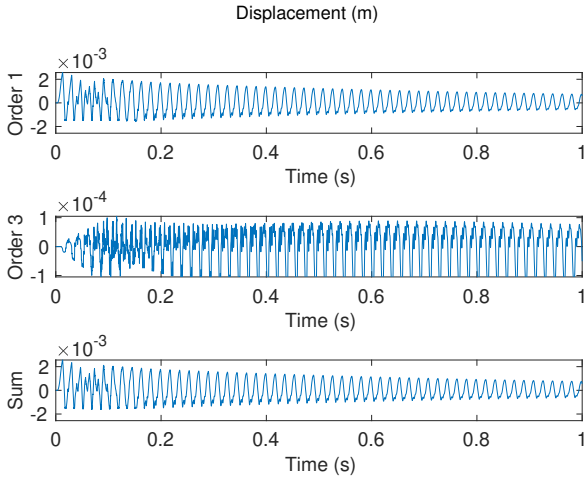

Figure 12: Displacement of the string at interaction point $x_I = 0.7L$ for the first order output, third order and their sum.

4.4 Interaction between the string and the plate

In many string instruments, the vibrating string is in interaction with a plate or a membrane. Many configuration are possible since the interaction can be made through a bridge (e.g. piano, violin) or not (snares on a snare drum [35]). In order to keep a simple application example, interaction of a string rigidly connected to a plate in one point will be considered. Interaction between a string and a plate with a rigid connection can be seen as imposing a zero relative velocity between one point of the plate and one point of the string. The block-diagram of Fig. 15 presents the computation procedure. We will assume that the plate and the string do not interact anywhere else. The string is excited by the external force (15-16) and is connected to the plate at interaction point $x_{Is} = 0.7L$. The plate is not excited and is in interaction with the string at point $(0.37L_x, 0.37L_y)$.

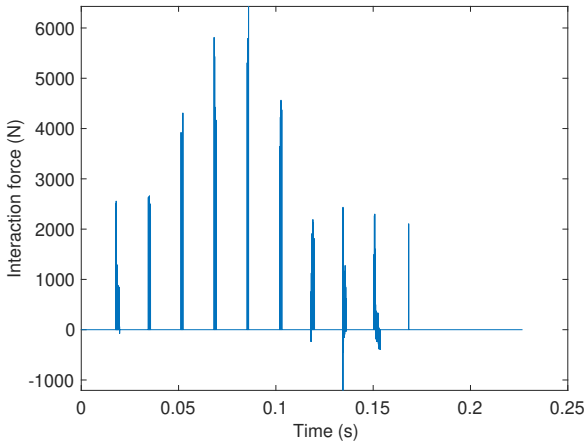

Figure 13: Interaction force due to the contact with the obstacle.

String and plate velocities at the interaction point are shown in Fig. 16a, at order 1, order 3 and their sum. On the last line the equal velocities constraint seems to be respected. This is verified in Fig. 16b where the relative velocity between the plate and the string is plotted. The exchange of energy between the two resonators can alse be observed in Fig. 17 which present string and plate magnitude spectra (in point $0.17L$ of the string and ($0.6L_x$,$0.6L_y$) for the plate). The three first eigenfrequencies of the string (55, 110 and 165 Hz) are visible at the same magnitude that the surrounding eigenfrequencies of the plate. For the case of the string, the interaction with the plate dynamics is also visible with five first eigenfrequencies of the plate between 37 and 110 Hz.

The order 3 response presented in Fig. 16a is very low in the case of the string whereas for the plate it has the same magnitude than the linear response. This can be seen more precisely in Fig. 17 where for the frequency of 55 Hz (first eigenfrequency of the string) the order 3 response of the plate have a magnitude of more than 50 dB. Readers interested in more general comments about coupling between a string and a plate can find more informations in [36, p. 282].

4.5 Computation cost

The main interest of the presented approach is to use a low cost formalism to simulate the dynamics of nonlinear systems. The choice to compute interactions using the inverse Volterra kernels allows to keep this advantage since no iterations are necessary to compute the output at one time step. On a recent laptop with a Intel Core i9, the case of a velocity constraint on one string, one second of sound with a constraint is computed in less than a second without any optimisation. The number of floating points operations is detailed in table 2 for simulation of the direct and inverse problems described in section 4.1.

5 Conclusion

The paper has introduced the sound synthesis based on nonlinear physical models described by their Volterra series and their interactions. Simulation of the dynamics of each resonator for known excitation is computed at low cost using their Volterra kernels. This work allows to design and compute interactions between these resonators using the inverse of their Volterra kernels in order to determine at each time step the interaction force. A structure of simulation and an algorithm are provided and differents applications for a single resonator or for coupling between two resonators are presented. Desired interactions are globally respected, however the case of collisions and constraints on the displacement reveals the limits of this approach and the need to consider an appropriate formalism such

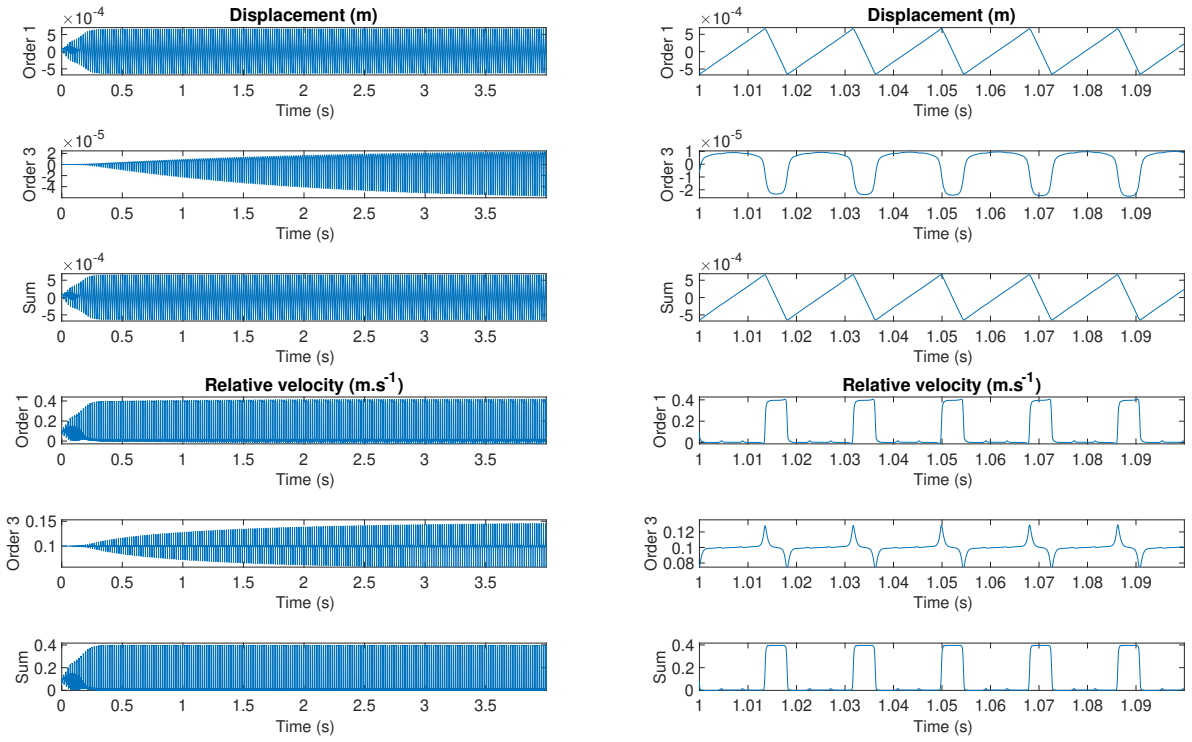

Figure 14: Self-oscillations of the string at the bowing point: Transverse displacement and relative velocity $v_r = v_B - v(x_I, t)$ at the bowing point for order one, three and their sum.

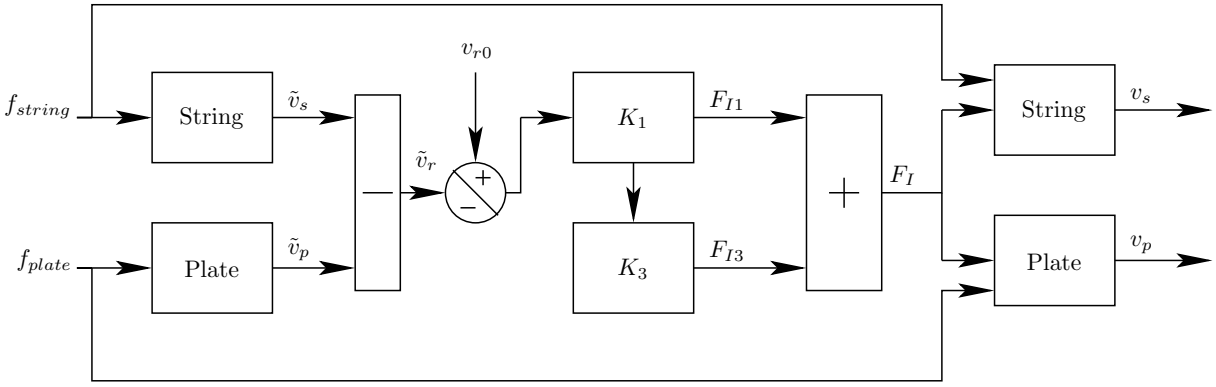

Figure 15: Block-diagram describing the computation of the dynamics of a string and a plate models in interaction. "String" and "plate" blocks compute respectively the dynamics of a string and a plate until order 3 using their respective Volterra kernels. v_{r0} is the desired relative velocity between the two systems. The difference of relative velocity $v_{r0} - \tilde{v}_r$ is the input of the inverse problem described by kernels K_n. The interaction force F_I computed is applied to both systems with opposite sign.

as nonsmooth dynamics. Moreover these results are limited by the hypotheses of Volterra series. The convergence has not been studied in this paper and is not guaranteed since the excitation and interaction forces should be lower than the radius of convergence of the series. Results on convergence for partial differential equations can be found in [37] and [38].

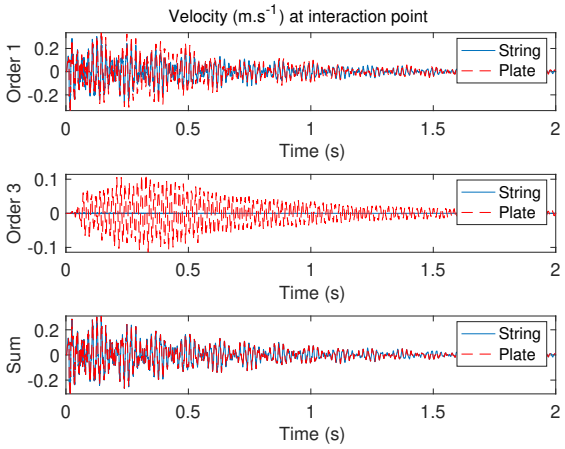

(a) Velocities of the plate and the string at order 1, 3 and their sum.

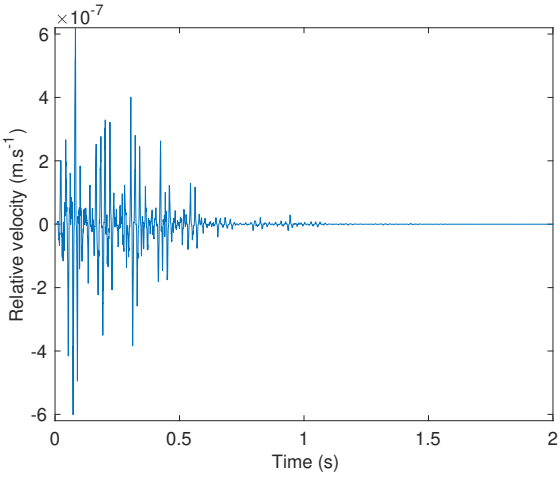

(b) Relative velocity between the plate and the string.

Figure 16: Velocities of the string and the plate at their interaction point. The interaction can be verified on the figure (b) which plots the relative velocity, i.e. the difference between the plate velocity and the string velocity.

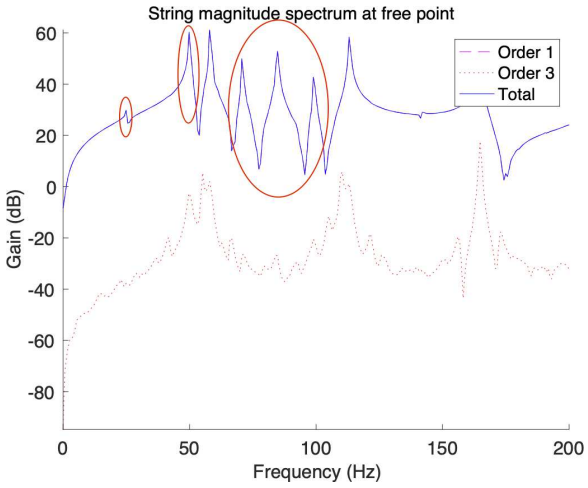

(a) String spectrum at point $x_{obs} = 0.17L$.

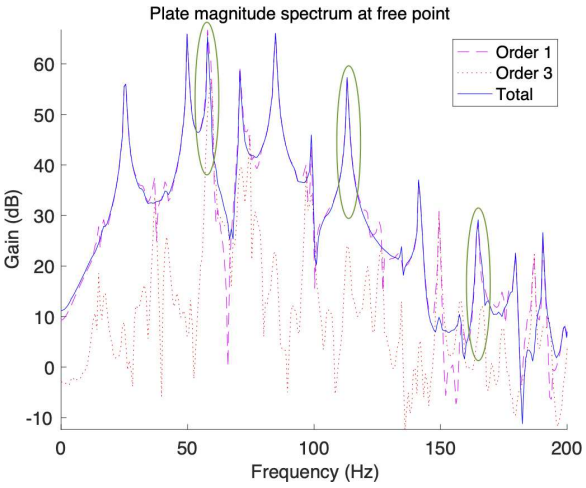

(b) Plate spectrum at point $(0.6L_x, 0.6L_y)$.

Figure 17: Spectrum magnitude of (a) the string at observation point $0.17L$; (b) the plate at observation point $(0.6L_x, 0.6L_y)$. Exchange of energy between the two systems is confirmed by the presence of the plate eigenfrequencies (highlighted in red) in the string signal and the presence of the string eigenfrequencies (in green) in the plate signal.

Acknowledgements

This research did not receive any specific grant from funding agencies in the public, commercial, or not-for-profit sectors.

	linear approx.: $N=1$, $o(\epsilon^0)$	third order approx.: $N=3$, $o(\epsilon^1)$
N^+	$K(N_q^+ + N_x) - N_x$	$K\left(2N_q^+ + N_x + 2\right) - N_x - 1$
$N^\times$	$K(N_q^\times + N_x)$	$K(2N_q^\times + N_x + 3) - 1$
N^{flops}	$K(N_q^{flops} + 2N_x) - N_x$	$K(2N_q^{flops} + 2N_x + 5) - N_x$
	linear approx. with interaction: $N=1$, $o(\epsilon^0)$	third order approx. with interaction: $N=3$, $o(\epsilon^1)$
N^+	$K(N_q^+ + N_x + 3) - N_x - 1$	$K(2N_q^+ + N_x + 13) - N_x - 1$
$N^\times$	$K(N_q^\times + N_x + 3) + 1$	$K(2N_q^\times + N_x + 21) + 2$
N^{flops}	$K(N_q^{flops} + 2N_x + 6) - N_x$	$K(2N_q^{flops} + 2N_x + 34) - N_x + 1$

Table 2: Number of floating point operations to compute the output of the direct problem (from [9]) and of the string interaction problem described in section 4.1 with K modes, at a given time time step, for N_x observation points. Using simulation algorithm described in Eq. (20), simulation of each filter requires $N_q^+ = 4$ sums and $N_q^\times = 6$ products.

A Reminder on the linear problem: modal sound synthesis

This section will remind the paradigm of modal sound synthesis based on linear physical models (A.1) and a definition of nonlinear interactions between linear resonators described in the modal formalism (A.2).

A.1 The direct problem: Green formalism and modal decomposition

Consider the case of a dimensionless linear wave propagation modelled by

$$\frac{\partial^2 u(x,t)}{\partial t^2} + \alpha \frac{\partial u(x,t)}{\partial t} - c^2 \Delta u(x,t) = f(x,t), \tag{18}$$

with a fluid damping α, a celerity c, the Dirichlet boundary conditions

$$u(0,t) = u(1,t) = 0,$$

and the initial conditions

$$u(x,0) = \frac{\partial u(x,0)}{\partial t} = 0.$$

The solution u of this problem is defined by the convolution

$$u(x,t) = \int_{\Omega \times \mathbb{R}^+} g(x,t;\xi,\tau) f(\xi,\tau) \mathrm{d}\xi \mathrm{d}\tau, \tag{19}$$

where f is the input force applied to the system and g is the Green function, i.e. the solution of Eq. (18) for a Dirac pulse input.

Given a modal decomposition $u(x,t) = \sum_{k=1}^{K} u^{[k]}(t) e_k(x)$ (with $e_k(x) = \sqrt{2}\sin(k\pi x)$), the second order boundary value problem described in Eq. (18) can be written as a set[1] of first order differential equations for $k \in \{1, 2, \ldots, K\}$

$$\begin{cases} \mathbf{X}^{[k]}(t) = \left[\begin{array}{cc} u^{[k]}(t) & \frac{\mathrm{d}u^{[k]}(t)}{\mathrm{d}t} \end{array} \right]^T, \\ \dot{\mathbf{X}}^{[k]}(t) = \mathbf{A}^{[k]} \mathbf{X}^{[k]}(t) + \mathbf{B} f^{[k]}(t), \\ \mathbf{A}^{[k]} = \left[\begin{array}{cc} 0 & 1 \\ -c^2(k\pi)^2 & -\alpha \end{array} \right], \quad \mathbf{B} = \left[\begin{array}{c} 0 \\ 1 \end{array} \right], \end{cases}$$

[1] a modal truncation is performed in order to obtain a finite dimensional set.

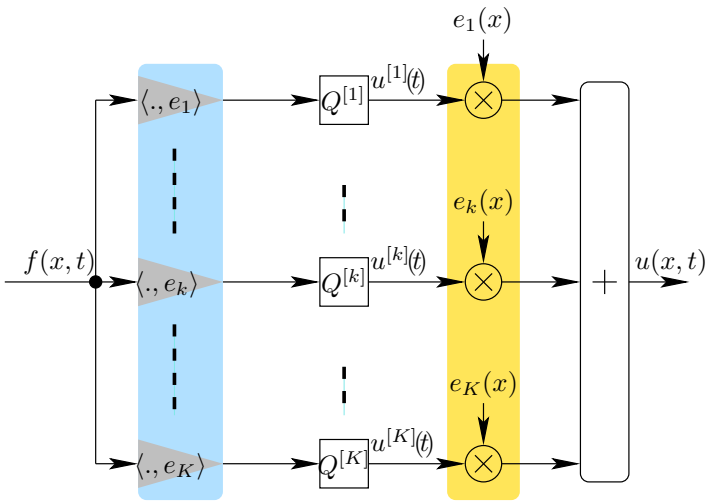

Figure 18: Structure of simulation of the dynamics of a resonator with a truncation at K modes.

where the matrix $\mathbf{A}^{[k]}$ captures the modal datas (eigen pulsation $\omega_k = c^2(k\pi)^2$, damping α) and $f^{[k]}$ are the modal forces. Using the exponential map, a solution can be formulated as (cf. [9])

$$\mathbf{X}^{[k]}(t) = \int_0^t \mathrm{e}^{\mathbf{A}^{[k]}(t-\tau)}\mathbf{B}f^{[k]}(\tau)\mathrm{d}\tau + \mathrm{e}^{\mathbf{A}^{[k]}t}\mathbf{X}^{[k]}(0),$$

which gives, after a time discretisation $t_h = ht_s$ (where t_s is the sampling period) and a zeroth order approximation of the input force, a recursive filter formula

$$\mathbf{X}^{[k]}(t_{h+1}) = \mathrm{e}^{\mathbf{A}^{[k]}t_s}\mathbf{X}^{[k]}(t_h) + \mathbf{B}_0^{[k]}f^{[k]}(t_{h+1}), \tag{20}$$

with $\mathbf{B}_0^{[k]} = -{\mathbf{A}^{[k]}}^{-1}\left[\mathbf{B} - \mathrm{e}^{\mathbf{A}^{[k]}t_s}\mathbf{B}\right]$. Technically, the computation of the exponential gives rise to a sound synthesis process described in Fig. 18 where $Q^{[k]}(s) = \frac{1}{s^2+\alpha s+\omega_k^2}$ are the filters associated to $\mathbf{A}^{[k]}$ and $\mathbf{B}$.

A.2 The interaction problem in discrete space and time domains

In this work interaction force written as $f_I(x,t) = \phi(x)F_I(t)$ will be considered where ϕ will represent the spatial distribution of the force. The general idea is to compute an interaction force in one point x_I (i.e. with $\phi(x) = \delta(x_I - x)$) from a given value of displacement or velocity, i.e. to solve an inverse problem. In order to do so, the solution in discrete time and space will be written as a sum between memory effects (inertia and elasticity) $\tilde{v}$ and a term related to the instantaneous force f_I

$$v(x_i,t) = \tilde{v}(x_i,t) + \frac{\partial g(x_i,x_i,t)}{\partial t} f_I(x_i,t),$$

which becomes in the discrete time and space domains

$$v(x_i,t) = \mathbf{C}\sum_{k=1}^{K}\left(\mathrm{e}^{\mathbf{A}^{[k]}t_s}\mathbf{X}^{[k]}(t_h) + \mathbf{B}_\phi^{[k]}F_I(t_{h+1})\right)e_k(x_i),$$

where $\mathbf{C} = \begin{bmatrix} 0 & 1 \end{bmatrix}$ and $\mathbf{B}_\phi^{[k]} = \phi^{[k]}\mathbf{B}_0^{[k]}$. Imposing a value v_0 to the velocity, the interaction force F_I can be computed by

$$F_I(t) = \frac{v_0 - \mathbf{C}\sum_{k=1}^{K}\mathrm{e}^{\mathbf{A}^{[k]}t_s}\mathbf{X}^{[k]}(t_h)e_k(x_i)}{\mathbf{C}\sum_{k=1}^{K}\mathbf{B}_\phi^{[k]}e_k(x_i)}. \tag{21}$$

In the the case of two resonators, the interaction definition will involve relative velocity between the two systems. This contact interaction can be permanent (e.g. adhere interaction) or not (e.g. strike interaction).

The relative velocity between the considered systems A and B, writes

$$\begin{aligned} v_r(t) &= v_A(x_A,t) - v_B(x_B,t), \\ &= \tilde{v}_A(x_A,t) - \tilde{v}_B(x_B,t) + \frac{\partial g^A(x_A,x_A,t)}{\partial t} f_I(x_A,t) - \frac{\partial g^B(x_B,x_B,t)}{\partial t} f_I(x_B t), \end{aligned}$$

which becomes

$$\begin{aligned} v_r(t) &= \mathbf{C} \sum_{k=1}^{K} \left(e^{\mathbf{A_A}^{[k]} t_s} \mathbf{X}_A^{[k]}(t_h) + \mathbf{B}_{\phi_A}^{[k]} F_{I_A}(t_{h+1}) \right) e_k^A(x_A), \\ &\quad - \left(e^{\mathbf{A_B}^{[k]} t_s} \mathbf{X}_B^{[k]}(t_h) + \mathbf{B}_{\phi_B}^{[k]} F_{I_B}(t_{h+1}) \right) e_k^B(x_B). \end{aligned}$$

Knowing, that $F_{I_A} = -F_{I_B}$ the general formulation of the interaction force is

$$F_{I_A}(t) = \frac{v_r - \mathbf{C} \sum_{k=1}^{K} \left(\mathrm{e}^{\mathbf{A_A}^{[k]} t_s} \mathbf{X}_A^{[k]}(t_h) - \mathrm{e}^{\mathbf{A_B}^{[k]} t_s} \mathbf{X}_B^{[k]}(t_h) \right) e_k(x_i)}{\sum_{k=1}^{K} \left(\mathbf{B}_{\phi_A}^{[k]} + \mathbf{B}_{\phi_B}^{[k]} \right) e_k(x_i)}.$$

B Volterra kernels of the dimensionless Berger plate model

One possibility to find the Volterra kernels (other methods can be found in e.g. [29, 39]) of a system is to write the cancelling system of its equation. Such a cancelling system is represented in Fig. 19 for the Berger plate model. It consists in assuming that the Volterra kernels $\{h_n\}$ are known. Therefore the output u is a solution which satisfies the partial differential equation (6) whose operators are represented in the block-diagrams, thus leading to an output $z = 0$ for all inputs f. More details can be found in [9].

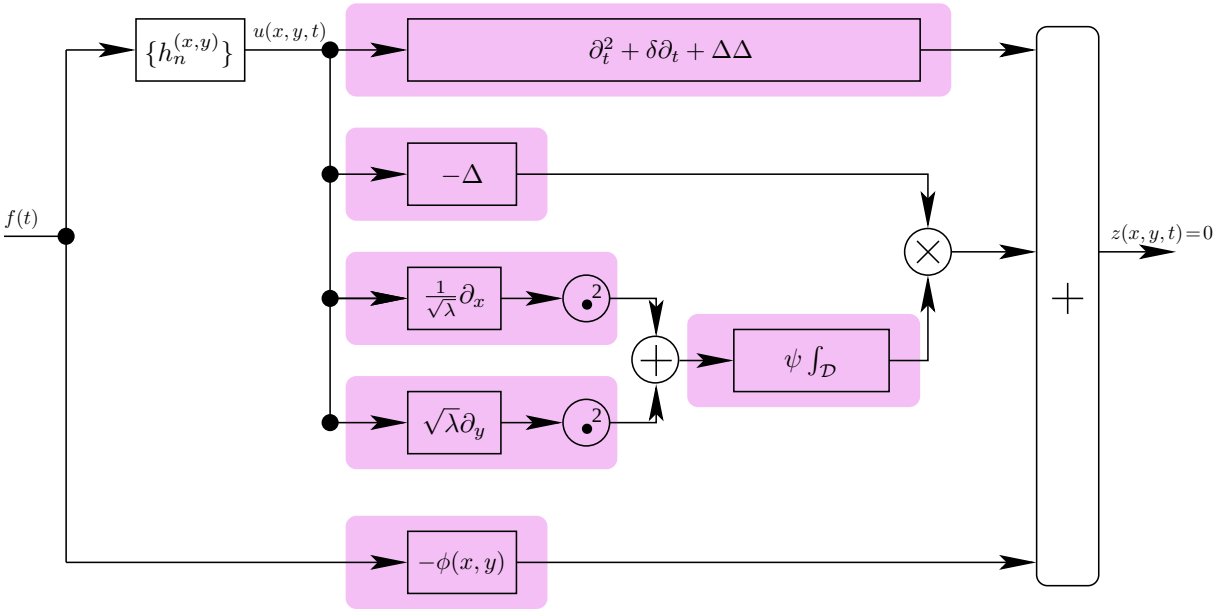

Figure 19: Block-diagram version of Eq. (6).

Using the block-diagram presented in Fig. 19 with the notation $\Delta = \frac{1}{\lambda}\partial_x^2 + \lambda\partial_y^2$ and the interconnections laws (2-4), the kernels equations can be derived in the Laplace domain for all order n:

$$\left[\widehat{\boldsymbol{s}}_{1:n}^2 + \left(\frac{1}{\lambda^2}\frac{\partial^4}{\partial x^4} + \lambda^2\frac{\partial^4}{\partial y^4} + 2\frac{\partial^4}{\partial x^2\partial y^2}\right) + \delta\widehat{\boldsymbol{s}}_{1:n}\right] H_n^{(x,y)}(\boldsymbol{s}) = E_n^{(x,y)}(\boldsymbol{s}), \tag{22}$$

with $E_1^{(x,y)}(s) = \phi(x,y)$,

$$E_n^{(x,y)}(\boldsymbol{s}) = \psi\int_{\mathcal{D}_0}\sum_{\substack{p,q,r<n\\ p+q+r=n}}\left(\frac{1}{\lambda}\frac{\partial H_p^{(x,y)}}{\partial x}\frac{\partial H_q^{(x,y)}}{\partial x} + \lambda\frac{\partial H_p^{(x,y)}}{\partial y}\frac{\partial H_q^{(x,y)}}{\partial y}\right)\mathrm{d}x\mathrm{d}y\left(\frac{1}{\lambda}\frac{\partial^2 H_r^{(x,y)}}{\partial x^2} + \lambda\frac{\partial^2 H_r^{(x,y)}}{\partial y^2}\right), \tag{23}$$

and the following boundary conditions

$$\begin{aligned}
H_n^{(x=0,y)}(\boldsymbol{s}) &= 0, & H_n^{(x=1,y)}(\boldsymbol{s}) &= 0,\\
H_n^{(x,y=0)}(\boldsymbol{s}) &= 0, & H_n^{(x,y=1)}(\boldsymbol{s}) &= 0,\\
\frac{\partial^2}{\partial y^2}H_n^{(x=0,y)}(\boldsymbol{s}) &= 0, & \frac{\partial^2}{\partial y^2}H_n^{(x=1,y)}(\boldsymbol{s}) &= 0,\\
\frac{\partial^2}{\partial x^2}H_n^{(x,y=0)}(\boldsymbol{s}) &= 0, & \frac{\partial^2}{\partial x^2}H_n^{(x,y=1)}(\boldsymbol{s}) &= 0.
\end{aligned}$$

Linear ordinary differential equation (22) can be solved using standard order reduction tools (finite elements method, finite differences, etc.). In this paper, modal decomposition will be used.

Modal decomposition Consider the Hilbert basis on the space $L^2(\Omega)$ where $\mathcal{D}_0 =]0,1[^2$

$$e_{kl}(x,y) = 2\sin(k\pi x)\sin(l\pi y), \tag{24}$$

which satisfies the boundary conditions. The projection of the Volterra kernels on the modes (k,l) will be denoted

$$H_n^{[kl]}(\boldsymbol{s}) = \int_{\mathcal{D}_0} H_n^{(x,y)}(\boldsymbol{s})e_{kl}(x,y)\mathrm{d}x\mathrm{d}y.$$

Projecting Eqs. (22)-(23) yields the following algebraic equations

$$\begin{aligned}
&\left\langle\left(\widehat{\boldsymbol{s}}_{1:n}^2 + \delta\widehat{\boldsymbol{s}}_{1:n} + \frac{1}{\lambda^2}\frac{\partial^4}{\partial x^4} + \lambda^2\frac{\partial^4}{\partial y^4} + 2\frac{\partial^4}{\partial x^2\partial y^2}\right) H_n^{(x,y)}, e_{kl}\right\rangle = \left\langle E_n^{(x,y)}, e_{kl}\right\rangle,\\
&\left(\widehat{\boldsymbol{s}}_{1:n}^2 + \delta\widehat{\boldsymbol{s}}_{1:n} + \frac{k^4\pi^4}{\lambda^2} + \lambda^2 l^4\pi^4 + 2k^2l^2\pi^4\right) H_n^{[kl]}(\boldsymbol{s}) = E_n^{[kl]}(\boldsymbol{s}),
\end{aligned}$$

leading to the following recurrent expression of the Volterra kernels

$$H_n^{[kl]}(\boldsymbol{s}) = Q^{[kl]}(\boldsymbol{s})E_n^{[kl]}(\boldsymbol{s}),$$

with

$$\begin{aligned}
Q^{[kl]}(\boldsymbol{s}) &= \left(\widehat{\boldsymbol{s}}_{1:n}^2 + \delta\widehat{\boldsymbol{s}}_{1:n} + \frac{k^4\pi^4}{\lambda^2} + \lambda^2 l^4\pi^4 + 2k^2l^2\pi^4\right)^{-1},\\
E_1^{[kl]}(s) &= \langle\phi, e_{kl}\rangle(x,y),
\end{aligned}$$

and

$$
\begin{aligned}
E_n^{[kl]}(\boldsymbol{s}) &= \psi\Bigg\langle \int_{\mathcal{D}} \sum_{p,q,r} \left(\frac{1}{\lambda} \frac{\partial H_p^{(x,y)}}{\partial x} \frac{\partial H_q^{(x,y)}}{\partial x} + \lambda \frac{\partial H_p^{(x,y)}}{\partial y} \frac{\partial H_q^{(x,y)}}{\partial y} \right) \mathrm{d}x\mathrm{d}y \\
&\quad \left(\frac{1}{\lambda} \frac{\partial^2 H_r^{(x,y)}}{\partial x^2} + \lambda \frac{\partial^2 H_r^{(x,y)}}{\partial y^2} \right), e_{kl} \Bigg\rangle, \\
E_n^{[kl]}(\boldsymbol{s}) &= -\psi\pi^4 (\frac{k^2}{\lambda} + l^2\lambda) \sum_{p,q,r} \sum_{(m,n)} H_p^{[mn]} H_q^{[mn]} \left(\frac{m^2}{\lambda} + n^2\lambda \right) H_r^{[kl]}, \\
E_n^{[kl]}(\boldsymbol{s}) &= \gamma_{kl} \sum_{p,q,r} \sum_{(m,n)} H_p^{[mn]} H_q^{[mn]} \left(m^2 + n^2\lambda^2 \right) H_r^{[kl]},
\end{aligned}
$$

with $\gamma_{kl} = \psi \frac{-\pi^4(k^2+l^2\lambda^2)}{\lambda^2}$.

References

[1] V. Välimäki, J. Pakarinen, C. Erkut, M. Karjalainen, Discrete-time modelling of musical instruments, Rep. Prog. Phys. 69 (1) (2005) 1–78. doi:10.1088/0034-4885/69/1/r01.

[2] S. Bilbao, J. O. Smith, Energy-conserving finite difference schemes for nonlinear strings, Acta Acust. united with Acust. 91 (2) (2005) 299–311.
URL http://www.ingentaconnect.com/content/dav/aaua/2005/00000091/00000002/art00012

[3] S. Bilbao, Numerical Sound Synthesis, Wiley-Blackwell, 2009. doi:10.1002/9780470749012.

[4] J. D. Morrison, J.-M. Adrien, MOSAIC: A framework for modal synthesis, Comput. Music J. 17 (1) (1993) 45. doi:10.2307/3680569.

[5] C. Cadoz, A. Luciani, J.-L. Florens, Responsive Input Devices and Sound Synthesis by Stimulation of Instrumental Mechanisms: The Cordis System, Comput. Music J. 8 (3) (1984) 60–73. doi:10.2307/3679813.

[6] J. L. Kelly, C. C. Lochbaum, Speech synthesis, in: Proc. 4th Int. Congr. Acoustics, Copenhagen, Denmark, 1962, pp. 1–4.

[7] J. O. Smith, Physical audio signal processing for virtual musical instruments and digital audio effects, online book at https://ccrma.stanford.edu/~jos/, Center for Computer Research in Music and Acoustics (CCRMA), Stanford University (2010).

[8] C. Desvages, S. Bilbao, Two-polarisation physical model of bowed strings with nonlinear contact and friction forces, and application to gesture-based sound synthesis, Appl. Sciences 6 (5) (2016) 135. doi:10.3390/app6050135.

[9] T. Hélie, D. Roze, Sound synthesis of a nonlinear string using Volterra series, J. Sound Vib. 314 (1-2) (2008) 275–306. doi:10.1016/j.jsv.2008.01.038.

[10] D. Roze, T. Hélie, Introducing a Green-Volterra series formalism to solve weakly nonlinear boundary problems: application to Kirchhoff's string, J. Sound Vib. 333 (7) (2014) 2073–2086. doi:10.1016/j.jsv.2013.11.024.

[11] M. Ducceschi, C. Touzé, S. Bilbao, C. J. Webb, Nonlinear dynamics of rectangular plates: investigation of modal interaction in free and forced vibrations, Acta Mech. 225 (1) (2013) 213–232. doi:10.1007/s00707-013-0931-1.

[12] S. Bilbao, A. Torin, V. Chatziioannou, Numerical modeling of collisions in musical instruments, Acta Acust. united with Acust. 101 (1) (2015) 155–173. doi:https://doi.org/10.3813/AAA.918813.

[13] V. Chatziioannou, M. van Walstijn, Energy conserving schemes for the simulation of musical instrument contact dynamics, J. Sound Vib. 339 (2015) 262–279. doi:10.1016/j.jsv.2014.11.017.

[14] M. Ducceschi, S. Bilbao, C. Desvages, Modelling collisions of nonlinear strings against rigid barriers: Conservative finite difference schemes with application to sound synthesis, in: International Congress on Acoustics, Buenos Aire, Argentina, 2016.

[15] M. van Walstijn, S. Mehes, An explorative string-bridge-plate model with tunable parameters, in: 20th Conference of Digital Audio Effects, Edinburgh, United Kingdom, 2017.

[16] C. Issanchou, J.-L. Le Carrou, C. Touzé, B. Fabre, O. Doaré, String/frets contacts in the electric bass sound: Simulations and experiments, Appl. Acoust. 129 (2018) 217–228. doi:10.1016/j.apacoust.2017.07.021.

[17] N. Lopes, T. Hélie, A. Falaize, Explicit second-order accurate method for the passive guaranteed simulation of port-hamiltonian systems, in: IFAC-LHMNLC, Vol. 48, Elsevier BV, 2015, pp. 223–228. doi:https://doi.org/10.1016/j.ifacol.2015.10.243.

[18] M. Ducceschi, S. Bilbao, Non-iterative solvers for nonlinear problems: the case of collisions, in: 22nd Conference of Digital Audio Effects, Birmingham, United Kingdom, 2019.

[19] M. Ducceschi, S. Bilbao, S. Willemsen, S. Serafin, Linearly-implicit schemes for collisions in musical acoustics based on energy quadratisation, J. Acoust. Soc. Am. 149 (5) (2021) 3502–3516. doi:https://doi.org/10.1121/10.0005008.

[20] M. Ducceschi, S. Bilbao, Non-iterative, conservative schemes for geometrically exact nonlinear string vibration, in: Proceedings of the 23rd International Congress on Acoustics, Aachen, Germany, 2019.

[21] F. E. Udwadia, R. E. Kalaba, A new perspective on constrained motion, Proc. R. Soc. Lond. Ser. A: Math. Phys. Sci. 439 (1906) (1992) 407–410. doi:10.1098/rspa.1992.0158.

[22] F. E. Udwadia, R. E. Kalaba, Analytical Dynamics, Cambridge University Press, 2007.

[23] J. Antunes, V. Debut, Dynamical computation of constrained flexible systems using a modal Udwadia-Kalaba formulation: Application to musical instruments, J. Acoust. Soc. Am. 141 (2) (2017) 764–778. doi:https://doi.org/10.1121/1.4973534.

[24] J. Antunes, V. Debut, L. Borsoi, X. Delaune, P. Piteau, A modal Udwadia-Kalaba formulation for vibro-impact modelling of continuous flexible systems with intermittent contacts, Procedia Eng. 199 (2017) 322–329. doi:10.1016/j.proeng.2017.09.058.

[25] J.-T. Jiolat, J.-L. Le Carrou, J. Antunes, C. d'Alessandro, Modelling of sympathetic string vibrations in the clavichord using a modal Udwadia-Kalaba formulation, in: Model Validation and Uncertainty Quantification, Volume 3, Springer International Publishing, 2019, pp. 277–280. doi:10.1007/978-3-030-12075-7_32.

[26] C. Issanchou, V. Acary, F. Pérignon, C. Touzé, J.-L. Le Carrou, Nonsmooth contact dynamics for the numerical simulation of collisions in musical string instruments, J. Acoust. Soc. Am. 143 (5) (2018) 3195–3205. doi:https://doi.org/10.1121/1.5039740.

[27] M. Schetzen, Theory of pth-order inverses of nonlinear systems, IEEE Trans. Circuits Syst. 23 (5) (1976) 285–291. doi:10.1109/tcs.1976.1084219.

[28] B. Trévisan, K. Ege, B. Laulagnet, Étude de sensibilité des paramètres de table d'harmonie de piano sur la synthese a
in: 13ème Congrès Français d'Acoustique, CFA 2016 - VISHNO, Le Mans, France, 2016.
URL https://hal.archives-ouvertes.fr/hal-01316317

[29] W. Rugh, Nonlinear system theory: the Volterra/Wiener approach, Johns Hopkins University Press, Baltimore, 1981.

[30] F. Lamnabhi-Lagarrigue, Analyse des systèmes non linéaires, Hermès, Paris, 1994.

[31] H. M. Berger, A new approach to the analysis of large deflections of plates, Ph.D. thesis, California Institute of Technology (1954).

[32] J. Nowinski, H. Ohnabe, On certain inconsistencies in berger equations for large deflections of plastic plates, Int. J. of Mech. Sci. 14 (3) (1972) 165–170. doi:10.1016/0020-7403(72)90073-2.

[33] T. Hélie, Modélisation physique d'instruments de musique et de la voix : systèmes dynamiques, problèmes directs et
Habilitation à diriger des recherches, Université Pierre et Marie Curie, Paris (2013).
URL http://recherche.ircam.fr/anasyn/helie/hdr/HdR_ThomasHelie.pdf

[34] V. Acary, B. Brogliato, Numerical Methods for Nonsmooth Dynamical Systems, Springer Berlin Heidelberg, 2008. doi:10.1007/978-3-540-75392-6.

[35] S. Bilbao, Time domain simulation and sound synthesis for the snare drum, J. Acoust. Soc. Am. 131 (1) (2012) 914–925. doi:https://doi.org/10.1121/1.3651240.

[36] A. Chaigne, J. Kergomard, Acoustics of Musical Instruments, Springer New York, 2016. doi:10.1007/978-1-4939-3679-3.

[37] T. Hélie, B. Laroche, Computable convergence bounds of series expansions for infinite dimensional linear-analytic systems and application, Autom. 50 (9) (2014) 2334–2340. doi:10.1016/j.automatica.2014.07.011.

[38] T. Hélie, B. Laroche, Input/output reduced model of a damped nonlinear beam based on volterra series and modal decomposition with convergence results, Nonlinear Dyn. 105 (2021) 515–540. doi:https://doi.org/10.1007/s11071-021-06529-6.

[39] R. W. Brockett, Volterra series and geometric control theory, Autom. 12 (2) (1976) 167–176. doi:10.1016/0005-1098(76)90080-7.